Liu, J. and McInnes, C. R. (2018) Resonant space tethered system for lunar orbital energy harvesting. *Acta Astronautica*, 156, pp. 23-32. (doi:10.1016/j.actaastro.2018.08.037)

Resonant space tethered system for lunar orbital energy harvesting

Jiafu Liu,[a*] Colin R McInnes[b]
[a]*SUN YAT-SEN UNIVERSITY, Shenzhen, Guangdong, 518000, China*

[b]*University of Glasgow, Glasgow, G12 8QQ, United Kingdom*

Abstract: Using a space tether system attached to the Moon's surface can in principle lead to energy harvesting from the mechanical damping of the tether as it experiences elongational motion due to time-varying tidal forces. It is shown that such a tether system can in principle provide electricity generation for lunar infrastructure, although the power generated is modest relative to the scale of engineering required. First, the dynamics of the coupled planar elongation and librational motion is established for a massless, elastic and damped tether with a large tip-mass in the frame of the elliptic Earth-moon restricted three-body (EEMRTB) system. Equilibria at the natural L_2 point are obtained as reference positions to perform the analysis. The method of multiple scales is then used to obtain the steady state amplitude-frequency response by ordering key variables and parameters appropriately. The steady-state power output determined by the elasticity, length and damping of the tether is presented. Specific resonances for peaks of power output, together with corresponding resonance regions, are also investigated along with suggestions for tradeoffs among the key system parameters. Finally, the optimal damping for maximum power output is determined, together with the corresponding natural length and elasticity of the tether.

Keywords: Energy harvesting, Space tethered system, Resonances, Multiscale analysis.

[*] Corresponding author: liujiafuericking@163.com.

1. Introduction

Energy harvesting from the environment is a research topic of significant contemporary interest [1-3] with intensive research on the harvesting of mechanical energy from ambient vibrations [4, 5]. This paper will present a novel energy harvesting strategy using a damped space tether connected to an end mass and the surface of the Moon. As the tether is forced by time-varying tidal forces due to the eccentricity of the lunar orbit, a damping device at the base of the tether generates power which can be tapped to provide a source of electrical energy. Physically, energy will be extracted from the Moon's orbital motion (as is the case for terrestrial tides), however this is not apparent in the analysis provided since only the restricted three-body problem is considered where the lunar orbit is fixed. The strategy therefore provides a new approach to generating electrical energy for future human lunar activities, and can also by synergistic with other lunar tether applications for payload transport.

One can find comprehensive and detailed reviews of space tether systems in [6], covering momentum exchange and electrodynamic tethers, where the main focus is on propulsion and power generation from tethered space platforms. Energy and power can be generated by exploiting the ambient environment such as the local magnetic field using electrodynamic tethers [7], which have also been proposed to be used as a propulsion method for space debris de-orbiting [8]. The design, using numerical and experimental analysis, of momentum exchange tethers was performed in [9-12]. The method of multiple scales was also used for determining approximate analytical solutions to tether dynamics with weak nonlinearity [10]. Tether design and laboratory experiments were performed for scale models in [11]. The motorised momentum exchange tether (MMET) has also been proposed to transport payloads between the Earth and Moon [11-12].

Energy and power generation at the Moon is an imperative once large-scale human lunar activity is underway. The dynamics of tethered systems attached to the Moon's surface have been studied in the framework of the restricted three-body problem in [13-14]. In-plane and out-of-plane librations, rather than elastic elongational motion, were investigated and were controlled by adjusting the rigid tether's length in [13-14]. Concerning nonlinear approximations for the analysis of tethered systems, the method of multiple scales was used to provide analytical solutions for the in-plane libration and pitch motion of a main [15] and sub-satellite respectively [16]. Nonlinear internal resonance was also addressed. For a space tether energy harvesting system, it is expected that one may enhance the energy harvesting process by designing the harvester with such internal resonances.

One can refer to [17] to understand how nonlinearities in mechanical energy harvesting systems affect the performance of the harvesters. Specifically, the bandwidth of the nonlinear energy harvester can be wider than for linear systems.

The effect of internal resonance on harvesting vibrational energy with a broad bandwidth has been investigated for a 2-degree of freedom dynamical system [18]. The performance of this nonlinear harvester was verified analytically using both the method of multiple scales and experiment. A hybrid nonlinear harvester considering both internal resonance and bi-stability was designed with vibrational energy harvested within a relatively broad frequency spectrum [19]. The 2:1 internal resonance between the symmetric and horizontal mode was utilized to enhance energy harvesting from a portal frame structure [20]. The dynamic instability and internal resonance of a vertical beam with a tip mass were also exploited to improve the efficiency of the vibration harvester [21], with the improvement of power output verified experimentally. Moreover, there exists a 2:1 internal resonance for a single piezoelectric cantilever attached by a pendulum. The bandwidth of a harvester can thus be broadened and the effectiveness of such a system has been verified both numerically and experimentally [22]. The vibration of a cantilever beam can also be attenuated by mounting an oscillator constrained to move along the beam with internal resonance between the vibration and the oscillator’s motion [23]. This new concept indicated that one can exploit internal resonance to both damp vibration and perform energy harvesting effectively [23].

One can also design mechanical systems with bi-stable or multi-stable equilibria to enhance energy harvesting [24-25]. The large displacements obtained, and thus enhanced power generation, is dramatically increased utilizing snap-through features of bi-stable systems. Bi-stable buckled beams have been adopted as a component of harvesters [26-27]. It was also clarified and verified that bistable buckled beams can harvest vibrational energy within a much wider frequency band and that the power output was also larger than for monostable beams.

This paper proposes the use of a long taut tether attached to the Moon’s surface to harvest energy from the damped elongational motion of the massless tether. The external excitation of the tether system arises from time-varying gravitational tides, specifically from the small but finite eccentricity of the orbit of the Earth-Moon system. Rayleigh dissipation of the elongation oscillations of the tether due to a damper as its base will then be used to generate power and the key parameters of the system (e.g. natural length, elasticity and damping coefficient) will be selected based on nonlinear resonance analysis. The paper presents an interesting new approach to generate lunar energy that merely utilizes the time-varying tidal forces due to the elliptical orbit of the Earth-Moon system; but again the power generated is modest relative to the scale of engineering required. It is noted that there exists an extensive literature concerning the dynamics and control of space tether systems and nonlinear dynamical analysis of energy harvesters. However, the nonlinear dynamical analysis of a long elastic space tether system for application to energy harvesting has not been addressed to the author's knowledge. The paper will focus on this problem and perform a nonlinear analysis, as discussed.

The organization of the paper is as follows. In Section 2, the detailed configuration of the space tether system and related reference frames are presented. Then, the dynamics of the space tether system is detailed in Section 3, with planar elastic elongation and in-plane libration. Equilibria within the elliptic Earth-Moon restricted three-body (EEMRTB) system are then investigated as reference states to facilitate the analysis. In Section 4 the method of multiple scales is used to provide approximate analytical solutions to the problem. In Section 5, the power output of the system is determined by the natural length, elasticity and base damping coefficient of the space tether which is presented and discussed. In addition, the largest steady-state tension and strain within the tether system are also calculated as a key consideration for designing the tether-based energy harvester. Moreover, the optimal damping for maximizing power output is determined, together with the corresponding natural length and elastic coefficient. In Section 6, conclusions are presented based on an analysis of the results presented in the preceding sections and the future work is also proposed.

2. Configuration of the space tether system

A long, massless tether is connected to the Moon's surface with a counterweight mass *S* and damper at its base, as shown in Fig. 1. The EEMRTB system includes the Earth, Moon and tether tip mass *S*. The tether system's parameters such its natural length and damping coefficient should be selected to ensure that the tether system is taut, and in libration, rather slack or in rotation at all times. It can be noted that one should select the natural length of the tether larger than the distance between the Moon and the natural $L_{2/1}$ point, and a comparatively large damping coefficient should be adopted, to ensure that the tether is taut during operations. One should also check whether the tether is always taut using numerical methods.

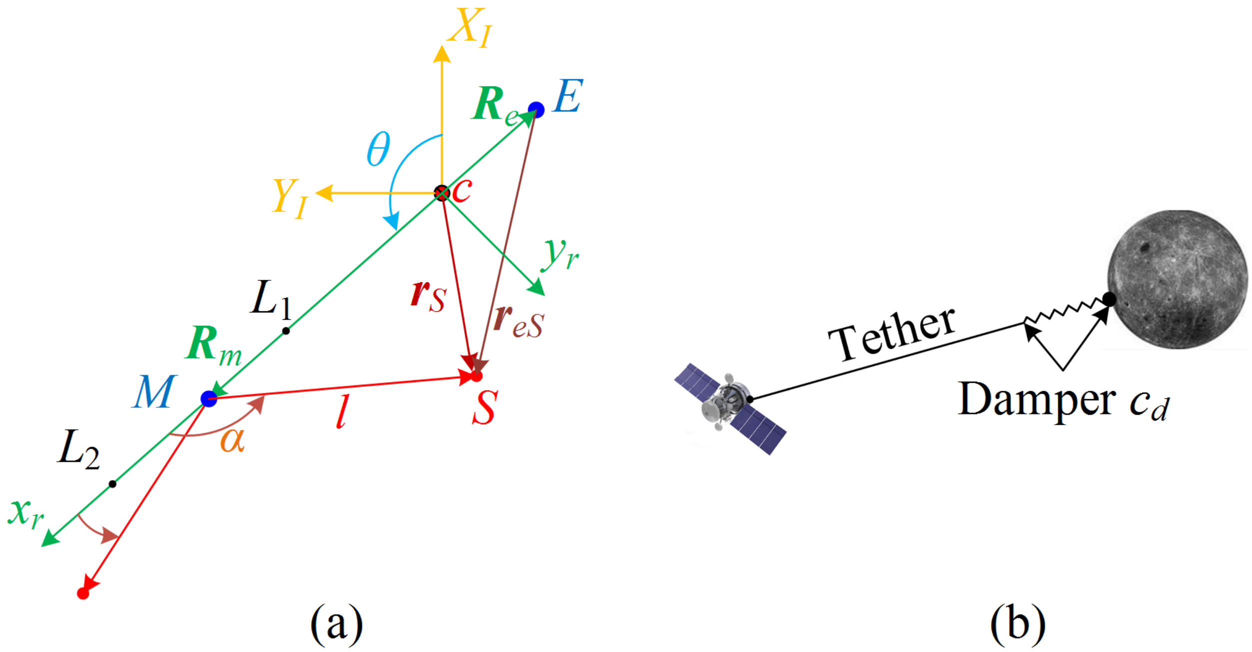

Fig. 1 **(a)** Space tether system in the EEMRTB system **(b)** Elastic tether and a damper at the base of the system

In Fig. 1, E and M denote the Earth and Moon respectively, and c is the common centre-of-mass. $\boldsymbol{R}_m$, $\boldsymbol{R}_e$ and $\boldsymbol{r}_S$ are the positions of the Earth, Moon and S relative to c respectively. Furthermore $\boldsymbol{l}$ and $\boldsymbol{r}_{eS}$ denote the positions of S relative to M and E respectively. Fixed and rotating reference frames are established, as shown in Fig. 1, denoted as $\boldsymbol{\pi}_I(cX_IY_IZ_I)$ and $\boldsymbol{\pi}_r(cx_ry_rz_r)$ respectively, where cX_I points to the orbit perigee, cZ_I points in the direction of the angular velocity of the Earth-Moon system about c, cx_r points from c to M and cz_r is coincident with cZ_I. Moreover, θ is the true anomaly of the Moon-Earth line rotating about c.

The tether is assumed to have a damper at its base which can be used to tap electrical power through the dissipation of the energy input to the tether due to the time-varying tidal forcing from the eccentricity of the Moon's orbit. One can envisage, for example, an array of piezoelectric elements close to the base of the tether at the lunar surface which dampen the elongational forcing of the tether and so generate electrical power. A simple Rayleigh model of the dissipation device with damping constant c_d will be used for illustration, as shown in Fig. 1(b).

In this paper the in-plane libration and elastic elongation of the massless tether (denoted as α and l in Fig. 1), and the orbital parameters are determined by α and l for this 2-dof system, driven by the gravitational tide between the Earth and Moon are considered. One can assert

$\alpha \in [0, \pi]$ when it is within the first and second quadrants, $\alpha \in [-\pi, 0]$ when it is within the third and fourth quadrants, both in $\boldsymbol{\pi}_r$ as shown in Fig. 1. The Lagrange method is utilized to obtain the coupled dynamics after deriving the kinetic energy, gravitational potential energy and elastic potential energy, and the Rayleigh dissipation function.

3. Dynamics of the space tether system

3.1 The dynamic modeling

As stated in the preceding section, one should derive the expressions for the relevant energies and dissipation function to arrive at dynamic equations utilizing the Lagrange method. To derive these energies for dynamic modeling, one should first define key position and velocity vectors.

For the EEMRTB system consisting of the Earth, Moon and S, the relative position vector between the two primaries pointing from the Earth to the Moon is denoted as $\boldsymbol{r}$ and is as follows.

$$\boldsymbol{r} = \begin{bmatrix} r \\ 0 \end{bmatrix}_r = \begin{bmatrix} \dfrac{a(1-e^2)}{1+ecos\theta} \\ 0 \end{bmatrix}_r \tag{1}$$

where a is the orbit semi-major axis and e is the eccentricity. The subscript r represents components in $\boldsymbol{\pi}_r$. It is evident that r is time-varying as e is nonzero. This is the cause of gravitational tidal forcing. It can be seen that $\boldsymbol{r}$ (also the subsequent position vectors) is two-dimensional as planar dynamics will be considered in this paper.

The position of S relative to c denoted as $\boldsymbol{r}_S$ is defined as follows by referring to Fig. 1.

$$\boldsymbol{r}_S = \boldsymbol{R}_m + \boldsymbol{l} = \begin{bmatrix} (1-\mu)r + lcos\alpha \\ lsin\alpha \end{bmatrix}_r = \begin{bmatrix} \mu_1 r + lcos\alpha \\ lsin\alpha \end{bmatrix}_r \tag{2}$$

where α is the pitch angle of the tether, measured from cx_r to $\boldsymbol{l}$ and $\mu \approx 1/81.3$ is mass ratio of the Moon to the Earth-Moon system, expressed as $m_m/(m_m + m_e)$, where m_m and m_e are the masses of the Moon and Earth respectively. We denote $\mu_1 = 1 - \mu$ as the mass ratio of the Earth.

The velocity of S is denoted as $\boldsymbol{v}_S$ and is as follows.

$$\boldsymbol{v}_S = \left.\frac{d\boldsymbol{R}_m}{dt}\right|_r + \left.\frac{d\boldsymbol{l}}{dt}\right|_r + \boldsymbol{\omega}_{rI} \times (\boldsymbol{R}_m + \boldsymbol{l}) = \begin{bmatrix} \mu_1 \dot{r} - l\dot{\alpha}sin\alpha - l\dot{\theta}sin\alpha + \dot{l}cos\alpha \\ \mu_1 r\dot{\theta} + l\dot{\alpha}cos\alpha + l\dot{\theta}cos\alpha + \dot{l}sin\alpha \end{bmatrix}_r \tag{3}$$

where $\left.\frac{\mathrm{d}(.)}{\mathrm{d}t}\right|_r$ represents a derivative with respect to time in frame $\boldsymbol{\pi}_r$ and $\boldsymbol{\omega}_{rI}$ is the angular velocity of the Earth- Moon system rotating about c, expressed here as $\dot{\theta}$ (where the overhead dot represents a time derivative).

The kinetic energy of S is denoted as T_S and is defined as

$$T_S = m\mu_1 rl\dot{\theta}^2 cos\alpha + \left(ml^2\dot{\theta}^2\right)/2 + \left(m\mu_1^2 r^2\dot{\theta}^2\right)/2 - \mu_1 mlr\dot{r}\dot{\theta}sin\alpha + \mu_1 mrl\dot{\alpha}\dot{\theta}cos\alpha + ml^2\dot{\alpha}\dot{\theta} \tag{4}$$

$$+ \mu_1 mr\dot{l}\dot{\theta}sin\alpha + (m\mu_1^2\dot{r}^2)/2 - \mu_1 ml\dot{r}\dot{\alpha}sin\alpha + \mu_1 m\dot{l}\dot{r}cos\alpha + (ml^2\dot{\alpha}^2)/2 + \left(m\dot{l}^2\right)/2$$

where *m* is the mass of *S*, adopted as 5×10^5 kg in this paper.

One can then calculate the gravitational energy U_g and elastic energy U_e of the system as

$$U_g = -\frac{\mu_m m}{|\boldsymbol{l}|} - \frac{\mu_e m}{|\boldsymbol{r} + \boldsymbol{l}|}, U_e = \frac{1}{2}k(l - l_0)^2 \tag{5}$$

where μ_m and μ_e are gravitational constants of the Moon and Earth respectively and k and l_0 are the elastic coefficient and natural length of the tether. In this paper, $l - l_0$ is always assumed to be non-negative to ensure that the tether is taut, so that the tether is always in tension.

The Rayleigh dissipation function Ψ_l for the tether's elongational motion is as follows.

$$\Psi_l = \left(c_d\dot{l}^2\right)/2 \tag{6}$$

where c_d is the damping coefficient and so Ψ_l is the power harvested during the forced motion. Again, it will be assumed that, for example, an array of piezoelectric elements close to the base of the tether at the lunar surface can be used to dampen the elongational forcing of the tether and so generate electrical power. The device is modelled simply by using the Rayleigh dissipation function in Eq. (6).

One can substitute Eqs. (4-6) into the following Lagrange equation to establish the dynamics of the space tether system using

$$\frac{d}{dt}\left(\frac{\partial L}{\partial \dot{\boldsymbol{q}}_n}\right) - \frac{\partial L}{\partial \boldsymbol{q}_n} - \boldsymbol{Q}_d = \boldsymbol{0} \tag{7}$$

where $L = T_S - U_g - U_e$, is the Lagrangian of the system, $\boldsymbol{q}_n = [l, \alpha]^T$, $\dot{\boldsymbol{q}}_n = \left[\dot{l}, \dot{\alpha}\right]^T$ and $\boldsymbol{Q}_d = -\left[\partial\Psi_l/\partial\dot{l}, 0\right]^T = \left[-c_d\dot{l}, 0\right]^T$ are the generalized displacements, velocities and damping forces respectively. The full nonlinear dynamics for the elongation and oscillation, or l and α degree of freedoms, are found to be.

$$\ddot{l} + \frac{c_d}{m}\dot{l} + \frac{k}{m}(l - l_0) - l\dot{\theta}^2 + \frac{\mu_m}{l^2} + \frac{\mu_e(l + rcos\alpha)}{(r^2 + l^2 + 2lrcos\alpha)^{3/2}} \tag{8}$$

$$-l\dot{\alpha}^2 - 2l\dot{\theta}\dot{\alpha} - \mu_1 r\dot{\theta}^2 cos\alpha + \mu_1 r\ddot{\theta}sin\alpha + 2\mu_1\dot{r}\dot{\theta}sin\alpha + \mu_1\ddot{r}cos\alpha = 0$$

$$l\ddot{\alpha} + 2\dot{l}\dot{\alpha} - \mu_1\dot{r}\dot{\alpha}cos\alpha - \mu_1 r\dot{\theta}\dot{\alpha}sin\alpha - \frac{\mu_e rsin\alpha}{(r^2 + 2lrcos\alpha + l^2)^{3/2}} \tag{9}$$

$$+\mu_1 r\dot{\theta}^2 sin\alpha + \mu_1 r\ddot{\theta}cos\alpha + 2\mu_1\dot{r}\dot{\theta}cos\alpha - \mu_1\ddot{r}sin\alpha + 2\dot{l}\dot{\theta} + l\ddot{\theta} = 0$$

One can analyze each term in the preceding two equations, e.g. the second and third terms of Eq. (8) correspond to damping and elastic accelerations. It is noteworthy that the coupled libration and elongation dynamics form a gyroscopic system as the problem is established in the rotating frame, and so the Coriolis acceleration is introduced naturally through the terms $2l\dot{\theta}\dot{\alpha}$ and $2\dot{l}\dot{\theta}$ in Eqs. (8-9).

However, it is not convenient to use the preceding dimensional dynamics to analyze the problem. The instantaneous distance between the Moon and Earth, denoted as *r*, the total mass M=m_e+m_m and reciprocal of the mean motion of the Earth and Moon are taken as the units of distance, mass, and time respectively. In addition, to simplify the analysis, the true anomaly θ is used as the independent variable instead of time *t* [28, 29]. The non-dimensional, non-linear coupled dynamics corresponding to the preceding dimensional dynamics can then be obtained as follows.

$$\frac{d^2\xi}{d\theta^2}+\frac{2\eta\varpi\left(\xi'+\frac{\xi esin\theta}{1+ecos\theta}\right)}{(1+ecos\theta)^2}-\xi\left(\alpha'\right)^2-2\xi\alpha'+\frac{\mu_1(\xi+cos\alpha)}{(1+ecos\theta)\left(1+\xi^2+2\xi cos\alpha\right)^{\frac{3}{2}}}+\frac{\varpi^2\left(\xi-\xi_0\right)}{(1+ecos\theta)^4}-\frac{\mu_1 cos\alpha}{1+ecos\theta}-\frac{\xi}{1+ecos\theta}+\frac{\mu}{\xi^2(1+ecos\theta)}=0 \tag{10}$$

$$\xi\alpha''+2(\alpha'+1)\xi'-\frac{\mu_1 sin\alpha}{(1+ecos\theta)(1+2\xi cos\alpha+\xi^2)^{\frac{3}{2}}}+\mu_1 sin\alpha-\mu_1\alpha' sin\alpha-\frac{\mu_1\alpha' esin\theta cos\alpha}{(1+ecos\theta)}-\frac{\mu_1 ecos\theta sin\alpha}{(1+ecos\theta)}=0 \tag{11}$$

In the preceding equations, $\xi=l/r$ is the dimensionless length of the tether and so $\xi_0=\frac{l_0(1+ecos\theta)}{a(1-e^2)}=(\zeta+\zeta ecos\theta)$ is the dimensionless natural length of the tether with $\zeta=\frac{l_0}{a(1-e^2)}$. It can be seen that the dimensionless natural length of the tether ξ_0 is time-varying as the time-varying instantaneous distance *r* is used as the unit of length but l_0 is a time-invariant dimensional natural length. Some definitions are introduced to simplify these expressions such as $\omega_n=\sqrt{k/m}, \eta=c_d/(2m\omega_n)$, $\omega_u=\sqrt{\mu_a/p^3}$ and $\varpi=\omega_n/\omega_u$. It is evident that ω_n is the natural frequency of the tether system, similar to a mass-spring system. Moreover, η is the damping ratio, ω_u is related to the mean angular rate of the Earth-Moon system, ϖ is a dimensionless angular rate used to describe the elasticity of the tether and p is the semi-latus rectum which can be expressed as $p = a(1-e^2)$. The prime now represents a derivative with respect to θ and $\mu_a = \mu_m + \mu_e$ is the summation of μ_m and μ_e.

The equations can be simplified as follows by taking e as small (neglect $O(e^2)$ terms) and θ related terms as excitations so that.

$$\xi'' + 2\eta\varpi\xi' + (\varpi^2 - 1)\xi - \xi(\alpha')^2 - 2\xi\alpha' + \frac{\mu}{\xi^2} + \frac{\mu_1(\xi + cos\alpha)}{(1 + \xi^2 + 2\xi cos\alpha)^{3/2}} - \mu_1 cos\alpha - \varpi^2\zeta$$

$$= \varpi^2\zeta ecos\theta + 4\varpi^2\xi ecos\theta - 4\zeta\varpi^2 ecos\theta - 2\eta\varpi\xi esin\theta + 4\eta\varpi\xi' ecos\theta$$

$$+ \frac{\mu_1(\xi + cos\alpha)ecos\theta}{(1 + \xi^2 + 2\xi cos\alpha)^{3/2}} - \xi ecos\theta + \frac{\mu ecos\theta}{\xi^2} - \mu_1 ecos\theta cos\alpha \tag{12}$$

$$\xi\alpha'' - \mu_1\alpha' sin\alpha + 2(\alpha' + 1)\xi' - \frac{\mu_1 sin\alpha}{(1 + 2\xi cos\alpha + \xi^2)^{3/2}} + \mu_1 sin\alpha$$

$$= \mu_1\alpha' esin\theta cos\alpha + \mu_1 ecos\theta sin\alpha - \frac{\mu_1 ecos\theta sin\alpha}{(1 + 2\xi cos\alpha + \xi^2)^{3/2}} \tag{13}$$

3.2 The equilibria and some simplifications

One can regard the eccentricity related terms in Eqs. (12, 13) as small perturbations since e is small. Then, equilibria can be calculated by taking e=0 in Eqs. (12, 13) as follows.

$$-\xi - \mu_1 cos\alpha + \frac{\mu}{\xi^2} + \frac{\mu_1(\xi + cos\alpha)}{(1 + \xi^2 + 2\xi cos\alpha)^{3/2}} + \varpi^2\xi - \varpi^2\zeta = 0 \tag{14}$$

$$\mu_1 sin\alpha - \frac{\mu_1 sin\alpha}{(1 + 2\xi cos\alpha + \xi^2)^{3/2}} = 0 \tag{15}$$

One can calculate the five natural Lagrange points by taking $\varpi = 0$ in the preceding two equations. These Lagrange points are shown in Fig. 2.

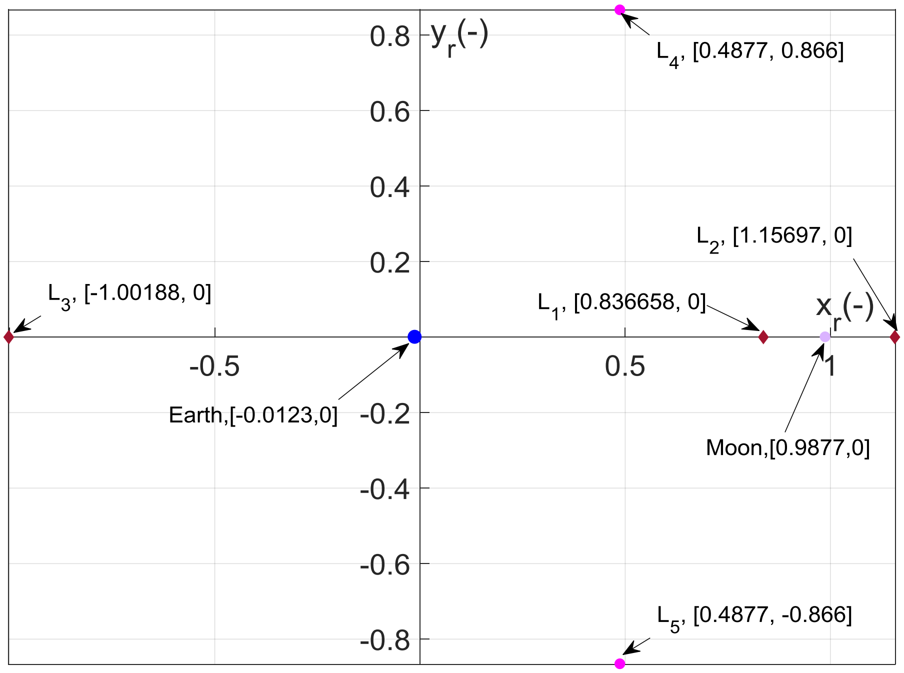

Fig. 2 The natural Lagrange points without considering the effect of an elastic tether.

It is well known that the collinear Lagrange points $L_{1,2,3}$ and the triangle Lagrange points $L_{4,5}$ as shown in Fig. 2, are unstable and stable respectively.

In principle, one will prefer to operate the tether system at the far side (i.e., the L_2 side) of the Moon as the largest elongated length of the tether can in principle be greater than the Earth-Moon distance, compared to a tether system operating on L_1 side of the Moon. In this paper, the collinear equilibrium point at L_2 is of interest and therefore α=0. Therefore one can arrive at the following equilibrium condition whereby.

$$-\mu_1 - \xi_e + \frac{\mu}{\xi_e^2} + \frac{\mu_1}{(\xi_e + 1)^2} + \varpi^2(\xi_e - \zeta) = 0 \tag{16}$$

where ξ_e is the equilibrium at the L_2 side of the Moon, determined by ϖ and ζ along with μ_1 and μ. Then, ξ_e can be numerically determined as long as ϖ and ζ are defined for a tether system within the Earth-Moon system. Morover, ζ can be further written as $\frac{nd}{p}$ with $p = a(1 - e^2)$ and $d \approx 6.485 \times 10^7$ m representing the semi-latus rectum and distance from the Moon to the natural L_2 point respectively (see Fig. 1). In this paper, the natural length of the tether l_0 is expressed as nd and n is then introduced to describe l_0, where n=1 corresponds to the tether tip mass located at L_2. The relationship between ξ_e, ϖ and n is shown in Fig. 3 (a) numerically, based on Eq. (16) and the subsequent discussion. In the analysis the natural length n of the tether should be larger than the distance between the Moon and natural L_2 point, meanwhile, smaller than 2 to save material and ensure that the solar gravitational perturbation is not large. The elastic coefficient of the tether should be selected to ensure the tip mass is not over far from the Moon. In conclusion, $n \in [1.1,2]$ and $\varpi \in [1.1,3.5]$ are chosen as preliminary parameter ranges.

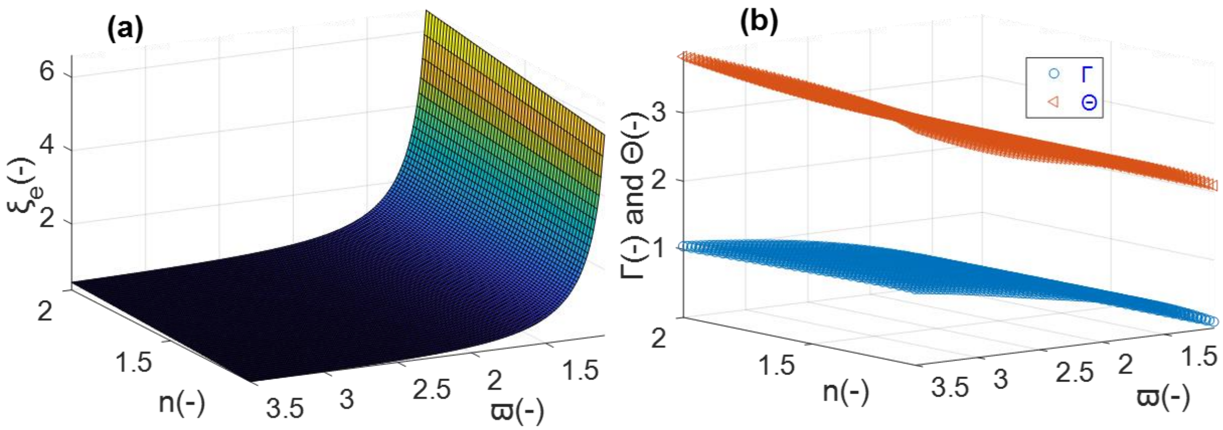

Fig. 3 **(a)** The equilibria determined by $\boldsymbol{\varpi}$ and n; **(b)** undamped natural frequencies.

The equilibria ξ_e obtained for each combination of ϖ and n will be used as reference positions for the analysis in the subsequent section. It is then straightforward to obtain the dimensional natural length of the tether l_0 and equilibria ξ_e as nd and $\xi_e a$ respectively. One can also obtain the expression for the dimensional elasticity of the tether k as $k = m\varpi^2 \frac{\mu_a}{a^3}$ by considering the discussion below Eq. (11). Therefore, the relationships between the dimensional and non-dimensional physical variables can be found from Fig. 3(a).

To perform a perturbation analysis for the nonlinear coupled dynamics with weak nonlinearity, one should introduce small but finite variables in Eqs. (12, 13) instead of ξ and α if necessary. In particular, a small but finite quantity $x = \delta/\xi_e = (\xi - \xi_e)/\xi_e$ is introduced as the fractional elongation of the tether in this paper. It is also assumed that α is a small but finite quantity. One can take x and α as two new independent variables. The following coupled nonlinear governing equations can then be obtained by substituting x, x' and x'' into Eqs. (12-13) and by taking x, x', α, α' and e as small quantities and neglecting the higher order terms so that.

$$\begin{aligned} &x'' + \omega_x^2 x - 2\alpha' + 2\eta\varpi x' - (\alpha')^2 - 2x\alpha' + C_{x1}x^2 + C_{x2}\alpha^2 + e[C_{x3}cos\theta + 2\eta\varpi sin\theta] \\ &\quad + e[C_{x4}xcos\theta - 4\eta\varpi x' cos\theta + 2\eta\varpi x sin\theta] = 0 \end{aligned} \tag{17}$$

$$\alpha'' + \omega_\alpha^2 \alpha + 2x' - \mu_1\xi_e^{-1}\alpha\alpha' + 2\alpha' x' - 2xx' + C_{\alpha1}\alpha x + e[C_{\alpha2}\alpha cos\theta - \mu_1\xi_e^{-1}\alpha' sin\theta] = 0 \tag{18}$$

with

$$\omega_x^2 = \varpi^2 - 1 - 2\mu\xi_e^{-3} - 2\mu_1(1+\xi_e)^{-3}, C_{x1} = 3\mu\xi_e^{-3} + 3\mu_1\xi_e(1+\xi_e)^{-4},$$

$$
\begin{gathered}
C_{x2}=(\mu_1\xi_e^{-1})/2+[1.53\mu_1(1+\xi_e)^{-4}]/2-[\mu_1\xi_e^{-1}(1+\xi_e)^{-3}]/2,\\
C_{x3}=1+\mu_1\xi_e^{-1}-\mu\xi_e^{-3}-\mu_1(1+\xi_e)^{-2}\xi_e^{-1}-\varpi^2\xi_e^{-1}\zeta-4\varpi^2\xi_e^{-1}(\xi_e-\zeta),\\
C_{x4}=1+2\mu\xi_e^{-3}+2\mu_1(1+\xi_e)^{-3}-4\varpi^2,\omega_\alpha^2=\mu_1\xi_e^{-1}-\mu_1\xi_e^{-1}(1+\xi_e)^{-3},\\
C_{\alpha 1}=\mu_1\xi_e^{-1}(1+\xi_e)^{-3}+3\mu_1(1+\xi_e)^{-4}-\mu_1\xi_e^{-1},C_{\alpha 2}=\mu_1\xi_e^{-1}(1+\xi_e)^{-3}-\mu_1\xi_e^{-1}
\end{gathered}
\tag{19}
$$

One can see that all coefficients $\omega_x^2,\omega_\alpha^2,C_{xi}(1,\cdots,4)\ and\ C_{\alpha j}(j=1,2)$ are determined by $\varpi\ and\ \zeta$ in Eq. (19). This indicates that the natural length and elasticity of the tether will strongly influence the dynamics of the tether system within the Earth-Moon system.

An approximate analytical analysis of Eqs. (17, 18) will now be performed and the method of multiple scales analysis used [30-31]. We rescale x,α and e as $x\leftrightarrow\varepsilon x,\alpha\leftrightarrow\varepsilon\alpha,e\leftrightarrow\varepsilon e$ with ε denoting a book-keeping device in the subsequent multiscale analysis. Here ε is merely used to order all the parameters and variables in the perturbation analysis. Then, Eqs. (17, 18) can be further simplified as follows.

$$
\begin{gathered}
x''+\omega_x^2x-2\alpha'+2\eta\varpi x'+e[C_{x3}cos\theta+2\eta\varpi sin\theta]\\
+\varepsilon[-(\alpha')^2-2x\alpha'+C_{x1}x^2+C_{x2}\alpha^2+eC_{x4}xcos\theta-4e\eta\varpi x'cos\theta+2e\eta\varpi xsin\theta]=0
\end{gathered}
\tag{20}
$$

$$
\alpha''+\omega_\alpha^2\alpha+2x'+\varepsilon[-\mu_1\xi_e^{-1}\alpha\alpha'+2\alpha'x'-2xx'+C_{\alpha1}\alpha x+eC_{\alpha2}\alpha cos\theta-e\mu_1\xi_e^{-1}\alpha' sin\theta]=0 \tag{21}
$$

Now that the underlying dynamics have been detailed the approximate analytic solution to the problem will be sought using the method of multiple scales.

4. Nonlinear analysis

One now assumes that the solutions to Eqs. (20, 21) can be expressed as follows.

$$
x(\theta,\varepsilon)=x_0(\theta_0,\theta_1)+\varepsilon x_1(\theta_0,\theta_1)+\cdots\ \ (a),\alpha(\theta,\varepsilon)=\alpha_0(\theta_0,\theta_1)+\varepsilon\alpha_1(\theta_0,\theta_1)+\cdots\ \ (b) \tag{22}
$$

and the related derivatives are therefore given by

$$
x'=\frac{\mathrm{d}x}{\mathrm{d}\theta}=\frac{\partial x_0}{\partial\theta_0}+\varepsilon\frac{\partial x_0}{\partial\theta_1}+\varepsilon\frac{\partial x_1}{\partial\theta_0},\alpha'=\frac{\mathrm{d}\alpha}{\mathrm{d}\theta}=\frac{\partial\alpha_0}{\partial\theta_0}+\varepsilon\frac{\partial\alpha_0}{\partial\theta_1}+\varepsilon\frac{\partial\alpha_1}{\partial\theta_0} \tag{23}
$$

$$
x''=\frac{\mathrm{d}^2x}{\mathrm{d}\theta^2}=\frac{\partial^2x_0}{\partial\theta_0^2}+2\varepsilon\frac{\partial^2x_0}{\partial\theta_1\partial\theta_0}+\varepsilon\frac{\partial^2x_1}{\partial\theta_0^2},\alpha''=\frac{\mathrm{d}^2\alpha}{\mathrm{d}\theta^2}=\frac{\partial^2\alpha_0}{\partial\theta_0^2}+2\varepsilon\frac{\partial^2\alpha_0}{\partial\theta_1\partial\theta_0}+\varepsilon\frac{\partial^2\alpha_1}{\partial\theta_0^2} \tag{24}
$$

where $\theta_0=\theta,\theta_1=\varepsilon\theta$. One can note that in Eqs. (22-24) the terms $O(\varepsilon^2)$ are now neglected. Substituting Eqs. (22-24) into Eqs. (20, 21) and equating the coefficients of $\varepsilon^0,\varepsilon$ on both sides, we obtain

ε^0 terms:

$$
\frac{\partial^2x_0}{\partial\theta_0^2}+\omega_x^2x_0-2\frac{\partial\alpha_0}{\partial\theta_0}+2\eta\varpi\frac{\partial x_0}{\partial\theta_0}=-e[C_{x3}cos\theta+2\eta\varpi sin\theta] \tag{25a}
$$

$$\frac{\partial^2\alpha_0}{\partial\theta_0^2}+\omega_\alpha^2\alpha_0+2\frac{\partial x_0}{\partial\theta_0}=0 \tag{25b}$$

ε^1 terms:

$$\frac{\partial^2 x_1}{\partial\theta_0^2}+\omega_x^2 x_1+2\eta\varpi\frac{\partial x_1}{\partial\theta_0}-2\frac{\partial\alpha_1}{\partial\theta_0}$$
$$=-2\frac{\partial^2 x_0}{\partial\theta_1\partial\theta_0}+2\frac{\partial\alpha_0}{\partial\theta_1}-2\eta\varpi\frac{\partial x_0}{\partial\theta_1}+\left(\frac{\partial\alpha_0}{\partial\theta_0}\right)^2+2x_0\frac{\partial\alpha_0}{\partial\theta_0}-C_{x1}x_0^2-C_{x2}\alpha_0^2-eC_{x4}x_0cos\theta$$
$$+4e\eta\varpi\frac{\partial x_0}{\partial\theta_0}cos\theta-2e\eta\varpi x_0 sin\theta \tag{26a}$$

$$\frac{\partial^2\alpha_1}{\partial\theta_0^2}+\omega_\alpha^2\alpha_1+2\frac{\partial x_1}{\partial\theta_0}$$
$$=-2\frac{\partial^2\alpha_0}{\partial\theta_1\partial\theta_0}-2\frac{\partial x_0}{\partial\theta_1}+\mu_1\xi_e^{-1}\alpha_0\frac{\partial\alpha_0}{\partial\theta_0}-2\frac{\partial\alpha_0}{\partial\theta_0}\frac{\partial x_0}{\partial\theta_0}+2x_0\frac{\partial x_0}{\partial\theta_0}-C_{\alpha1}\alpha_0x_0-eC_{\alpha2}\alpha_0cos\theta$$
$$+e\mu_1\xi_e^{-1}\frac{\partial\alpha_0}{\partial\theta_0}sin\theta \tag{26b}$$

The natural frequencies corresponding to undamped free vibration are obtained as follows by taking η and e equal to 0 in Eq. (25) so that.

$$\Gamma=\sqrt{\frac{c_0-\sqrt{c_0^2-4c_1}}{2}},\Theta=\sqrt{\frac{c_0+\sqrt{c_0^2-4c_1}}{2}} \tag{27}$$

with c_0 and c_1 as $c_0=\omega_\alpha^2+\omega_x^2+4, c_1=\omega_x^2\omega_\alpha^2$. It is evident that Γ and Θ are the undamped natural frequencies of the gyroscopic system. The dependence of Γ and Θ on the natural length and elasticity of the tether can be seen in Eq. (19) and Eq. (27) and illustrated in Fig. 3(b).

We now illustrate how Γ and Θ vary with ϖ and n in Fig. 3(b). In this paper, we select η larger than 1 to ensure that the space tether is in tension at all times for successful operations. On the contrary, the tether will lose tension and rotate when η is small. The solutions to Eq. (25) can then be presented as follows.

$$x_0=K_1(\theta_1)e^{(-\lambda_{1R}+\mathrm{i}\lambda_{1I})\theta_0}+\left[C_3(\theta_1)e^{-\lambda_{3R}\theta_0}\right]/2+\left[C_4(\theta_1)e^{-\lambda_{4R}\theta_0}\right]/2\underline{+ae^{\mathrm{i}\theta}}+\bar{K}_1(\theta_1)e^{(-\lambda_{1R}-\mathrm{i}\lambda_{1I})\theta_0}$$
$$+\left[C_3(\theta_1)e^{-\lambda_{3R}\theta_0}\right]/2+\left[C_4(\theta_1)e^{-\lambda_{4R}\theta_0}\right]/2\underline{+\bar{a}e^{-\mathrm{i}\theta}} \tag{28a}$$

$$\alpha_0=p_1K_1(\theta_1)e^{(-\lambda_{1R}+\mathrm{i}\lambda_{1I})\theta_0}+\left[p_2C_3(\theta_1)e^{-\lambda_{3R}\theta_0}\right]/2+\left[p_3C_4(\theta_1)e^{-\lambda_{4R}\theta_0}\right]/2\underline{+be^{\mathrm{i}\theta}}+\bar{p}_1\bar{K}_1(\theta_1)e^{(-\lambda_{1R}-\mathrm{i}\lambda_{1I})\theta_0}$$
$$+\left[p_2C_3(\theta_1)e^{-\lambda_{3R}\theta_0}\right]/2+\left[p_3C_4(\theta_1)e^{-\lambda_{4R}\theta_0}\right]/2\underline{+\bar{b}e^{-\mathrm{i}\theta}} \tag{28b}$$

where the complex function $K_1(\theta_1)$ is a function of θ_1, i is the unit pure imaginary number, C_3 and C_4 are real and the overhead bar represents the conjugate of a complex term. Then $-\lambda_{1R} + \mathrm{i}\lambda_{1I}$, $-\lambda_{3R}$ and $-\lambda_{4R}$ are the roots of the characteristic equations of Eq. (25). Moreover, p_{1-3} and a, b are presented as follows.

$$p_1 = -\omega_\alpha^{-2}[(-\lambda_{1R} + \mathrm{i}\lambda_{1I})^3 + 2\eta\varpi(-\lambda_{1R} + \mathrm{i}\lambda_{1I})^2 + (\omega_x^2 + 4)(-\lambda_{1R} + \mathrm{i}\lambda_{1I})]/2,$$
$$p_2 = -\omega_\alpha^{-2}[(-\lambda_{3R})^3 + 2\eta\varpi(-\lambda_{3R})^2 + (\omega_x^2 + 4)(-\lambda_{3R})]/2,$$
$$p_3 = -\omega_\alpha^{-2}[(-\lambda_{4R})^3 + 2\eta\varpi(-\lambda_{4R})^2 + (\omega_x^2 + 4)(-\lambda_{4R})]/2$$

$$a = \frac{[-(eC_{x3})/2 + e\eta\varpi\mathrm{i}](\omega_\alpha^2 - 1)}{(\omega_\alpha^2 - 1)(\omega_x^2 - 1) + 2\eta\varpi\mathrm{i}(\omega_\alpha^2 - 1) - 4}, b = \frac{(\mathrm{i}eC_{x3} + 2e\eta\varpi)}{(\omega_\alpha^2 - 1)(\omega_x^2 - 1) + 2\eta\varpi\mathrm{i}(\omega_\alpha^2 - 1) - 4}$$

The solution to Eq. (25) consists of a transient damped general solution corresponding to the first three terms in Eq. (28), with the steady-state particular solution corresponding to the fourth term in Eq. (28). By analyzing Eq. (28), it can be seen that the resonance region is near $\lambda_{1I} = 1$ as the single-frequency external force is a function of $e^{\mathrm{i}\theta}$ (where the frequency is unity).

We substitute the steady part of x_0 and α_0 into the second-order equations, i.e., Eq. (26), to obtain particular solutions without damped, transient solution as follows.

$$\frac{\partial^2 x_1}{\partial\theta_0^2} + \omega_x^2 x_1 + 2\eta\varpi\frac{\partial x_1}{\partial\theta_0} - 2\frac{\partial\alpha_1}{\partial\theta_0} = \Xi_1 e^{2\mathrm{i}\theta_0} + \Xi_2 + \bar{\Xi}_1 e^{-2\mathrm{i}\theta_0} + \bar{\Xi}_2 \qquad (29a)$$

$$\frac{\partial^2\alpha_1}{\partial\theta_0^2} + \omega_\alpha^2\alpha_1 + 2\frac{\partial x_1}{\partial\theta_0} = \Xi_3 e^{2\mathrm{i}\theta_0} + \Xi_4 + \bar{\Xi}_3 e^{-2\mathrm{i}\theta_0} + \bar{\Xi}_4 \qquad (29b)$$

where the constants $\Xi_{1,\ldots,4}$ are defined as

$$\Xi_1 = (-2b^2 + 4\mathrm{i}ab + 4\mathrm{i}be\eta\varpi - 2a^2C_{x1} - 2b^2C_{x2} + 2\mathrm{i}ae\eta\varpi - aeC_{x4})/2,$$
$$\Xi_2 = \left(2b\bar{b} + 4\mathrm{i}b\bar{a} + 4\mathrm{i}be\eta\varpi - 2a\bar{a}C_{x1} - 2b\bar{b}C_{x2} - 2\mathrm{i}ae\eta\varpi - aeC_{x4}\right)/2,$$
$$\Xi_3 = (+4ab - 2abC_{\alpha1} - beC_{\alpha2} + 2\mathrm{i}\xi_e^{-1}b^2\mu_1 + \xi_e^{-1}be\mu_1 + 4\mathrm{i}a^2)/2,$$
$$\Xi_4 = (-4b\bar{a} - 2b\bar{a}C_{\alpha1} - beC_{\alpha2} - \xi_e^{-1}be\mu_1)/2 \qquad (30)$$

One can arrive at the particular solutions to Eq. (29) as follows.

$$x_1 = \mathrm{Z}_1 e^{2\mathrm{i}\theta_0} + \mathrm{Z}_2 + \bar{\mathrm{Z}}_1 e^{-2\mathrm{i}\theta_0} + \bar{\mathrm{Z}}_2 \ (a), \alpha_1 = \mathrm{Z}_3 e^{2\mathrm{i}\theta_0} + \mathrm{Z}_4 + \bar{\mathrm{Z}}_3 e^{-2\mathrm{i}\theta_0} + \bar{\mathrm{Z}}_4 \ (b) \qquad (31)$$

where $\mathrm{Z}_1, \mathrm{Z}_2, \mathrm{Z}_3$ and Z_4 are given as

$$\mathrm{Z}_1 = \frac{(\omega_\alpha^2 - 4)\Xi_1 + 4\mathrm{i}\Xi_3}{[(\omega_\alpha^2 - 4)(-4 + \omega_x^2 + 4\mathrm{i}\eta\varpi) - 16]}, \mathrm{Z}_2 = \omega_x^{-2}\Xi_2, \mathrm{Z}_3 = \omega_\alpha^{-2}\Xi_4, \mathrm{Z}_4 = \frac{\Xi_3(-4 + \omega_x^2 + 4\mathrm{i}\eta\varpi) - 4\mathrm{i}\Xi_1}{[(\omega_\alpha^2 - 4)(-4 + \omega_x^2 + 4\mathrm{i}\eta\varpi) - 16]} \qquad (32)$$

One can then obtain the full solution to x as follows by substituting Eqs. (28a, 31a) into Eq. (22a).

$$x = x_0 + \varepsilon x_1 = ae^{\mathrm{i}\theta} + \mathrm{Z}_1 e^{2\mathrm{i}\theta} + \mathrm{Z}_2 + \bar{a}e^{-\mathrm{i}\theta} + \bar{\mathrm{Z}}_1 e^{-2\mathrm{i}\theta} + \bar{\mathrm{Z}}_2 \qquad (33)$$

One can arrive at the expression for l as follows by considering $x = \delta/\xi_e = (\xi - \xi_e)/\xi_e$ and $\xi = \frac{l}{r}$.

$$l = r\xi = (x+1)\xi_e r = (x+1)\xi_e \frac{a(1-e^2)}{1+ecos\theta} \tag{34}$$

The expression for dl/dt is then written as

$$\dot{l} = r\frac{d\xi}{dt} + \xi\frac{dr}{dt} = \frac{a(1-e^2)}{1+ecos\theta}\xi_e\frac{dx}{d\theta}\frac{d\theta}{dt} + (x+1)\xi_e\sqrt{\frac{\mu_a}{p}}esin\theta$$

$$= \frac{a(1-e^2)}{1+ecos\theta}\xi_e\frac{dx}{d\theta}\sqrt{\frac{\mu_a}{p^3}}(1+ecos\theta)^2 + (x+1)\xi_e\sqrt{\frac{\mu_a}{p}}esin\theta$$

$$= \frac{a(1-e^2)}{1+ecos\theta}\xi_e(-2asin\theta - 4\mathrm{Z}_1 sin2\theta)\sqrt{\frac{\mu_a}{p^3}}(1+ecos\theta)^2 + (x+1)\xi_e\sqrt{\frac{\mu_a}{p}}esin\theta \tag{35}$$

Finally, one can write the approximate analytical solution to power output as follows.

$$\Psi_l = \frac{\left(c_d \dot{l}^2\right)}{2} = \eta\sqrt{km}\left[\frac{a(1-e^2)}{1+ecos\theta}\xi_e(-2asin\theta - 4\mathrm{Z}_1 sin2\theta)\sqrt{\frac{\mu_a}{p^3}}(1+ecos\theta)^2 + (x+1)\xi_e\sqrt{\frac{\mu_a}{p}}esin\theta\right]^2 \tag{36}$$

One should note that the perturbation method (multiscale analysis) is valid and accurate for dynamics with weak nonlinearity, i.e., the nonlinear terms in Eqs. (17, 18) should be small compared to the linear terms. Otherwise, the perturbation method will be inaccurate.

5. Results

There are three important parameters for the tether system, i.e., n, ϖ and η. Analytical and numerical results will therefore be presented for various sets of n, ϖ and η to explore the parameter space of the problem. It is known that the frequency of the damped system is determined by n, ϖ and η, while the frequency of the external forcing is simply unity (1) in this paper. Therefore, one should select n, ϖ and η to make the frequency of the damped system of order unity to utilize the resonance of the forced tether system to generate power, again through the simple Rayleigh dissipation model. First, $n \in [1.1, 2]$, $\varpi \in [1.1, 2.5]$ and $\eta \in [2, 4]$ are selected to illustrate the performance of the lunar tether based energy harvester. Next, the parameter range η will be expanded from for $\eta \in [2, 4]$ to $\eta \in [2, 7]$ to explore the optimal damping with largest power output. One can expect the maximisation of power output from the harvesting mechanism when the parameters (n, ϖ and η) of the nonlinear harvester are selected to design the system to be within the resonant region of the parameter space. All numerical values used are summarized in Table. 1.

Table 1. Values for all parameters used in the analysis

Parameters	Values	Parameters	Values
μ	1/81.3	μ_e	3.986×10^{14}km^3/s^2
μ_1	80.3/81.3	μ_m	4.9028×10^{12}km^3/s^2
m	5×10^5kg	μ_a	4.035×10^{14}km^3/s^2
d	6.485×10^7m	m_e	5.965×10^{24}kg
a	3.84748×10^8m	m_m	7.349×10^{22}kg
e	0.0549006	M	6.03849×10^{24}kg
p	3.83588×10^8m	-	-

In this paper, the approximate analytical solutions are pursued utilizing the multiscale analysis method. The numerical solutions are also presented to validate the analytical results. The ode45 solver is used to perform the numerical calculations, based on an explicit Runge-Kutta (4,5) formula with the Dormand-Prince pair. In the solver, the maximal, minimal and initial step sizes are 5×10^{-3}, 1×10^{-5} and 1×10^{-5} respectively. The relative and absolute tolerances are both 1×10^{-5}. In this section, to demonstrate and discuss the results with clearer physical implications, we present the relations between the tether's dimensionless natural length (n), elasticity (ϖ) and damping (η), and dimensional natural length (l_0), elasticity (k) and damping (c_d) respectively. i.e., $l_0=(nd)=6.485\times10^7n$ m, $k = m\varpi^2 \frac{\mu_a}{a^3} = 3.54\times10^{-6}\varpi^2$ N/m and $c_d = 2m\sqrt{\frac{\mu_a}{a^3}}\varpi\eta \approx 2.66\varpi\eta$ N·s/m with $d\approx6.485\times10^7$ m, $m=5\times10^5$ kg, $\mu_a = \mu_e + \mu_m = 4.04\times10^{14}$ m^{3}s^{-2}and $a=3.84748\times10^8$ m. It can be seen that the dimensional damping c_d is determined by the dimensionless damping η and elasticity ϖ.

First, the validation of the approximate analytical solution will be verified by presenting and comparing the energy harvesting results using both analytical and numerical calculations as follows. The corresponding resonance region boundaries and the peak power curves are also presented. The boundary for useful power generation is selected as 15 kW (shown as the red and blue contours in Fig. 4, with the peak power contour indicated in black) and the damping is selected as $\eta=4$ (the dimensional damping c_d is $c_d = 10.6468\varpi$ N·s/m, determined by the dimensionless elasticity ϖ). There are no explicit reasons for selecting the boundary value 15 kW, but it is used for ease of illustration.

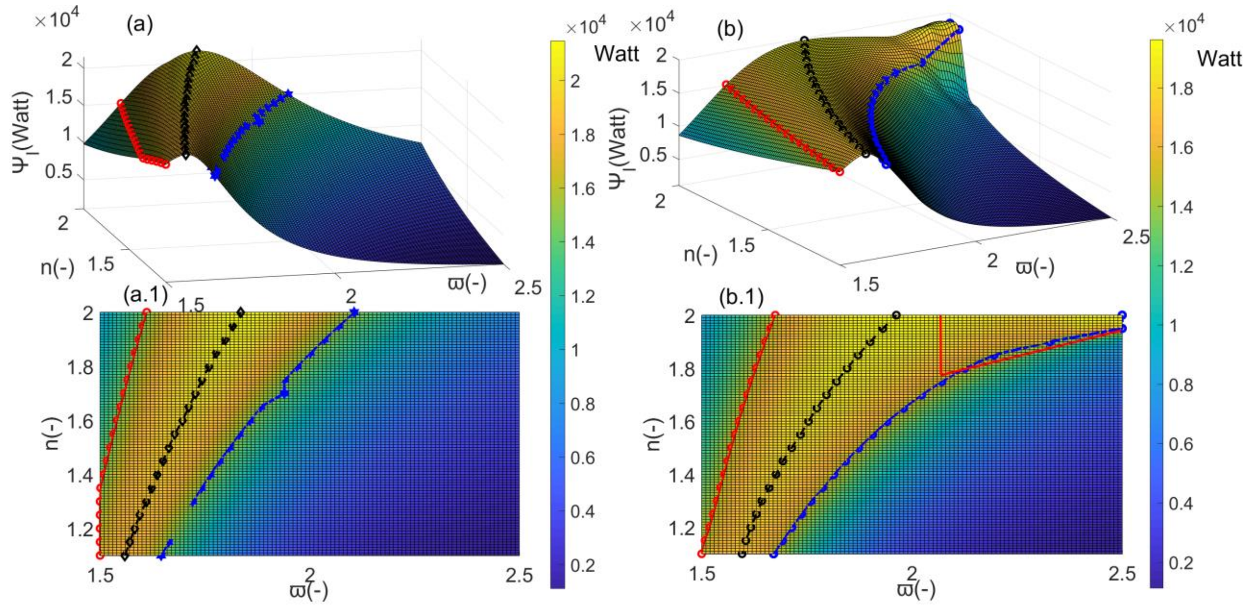

Fig. 4 Power output based on the analytical **(a, a.1)** and numerical **(b, b.1)** methods, the resonance regions are covered by the labelled curves.

First, it can be seen that the analytical solution (see Eq. (36)) agrees well with the numerical solution (which can be obtained numerically using Eqs. (6, 8 and 9)) both quantitatively and qualitatively, except the conditions when both the dimensionless natural length and elasticity of the tether denoted as n and ϖ adopt large values (n approaches 2 and ϖ approaches 2.5, i.e., the top-right region indicated by a solid red box in Fig. 4(b.1). It can be seen that the dimensional natural length and elasticity denoted as l_0 and k are 1.297×10^8 m and 2.2125×10^{-5} N/m accordingly). Specifically, the actual resonance regions seem larger than those predicted by the analytical method, as can be seen from the results in Fig. 4(a.1) and (b.1). It is suggested that one should design the energy harvester with large resonance regions to ensure robustness. For example, a harvester with n=2 and $\varpi\approx2$ (the dimensional natural length, elasticity and damping are l_0=1.297×10^8 m, k=1.416×10^{-5} N/m and c_d=21.29359259 N·s/m accordingly) will have good performance, as can be seen from Fig. 4(b.1) since the power output will be maximum as the system is resonant. Moreover, the power output is insensitive to n and ϖ near n=2 and $\varpi\approx2$. Again, the harvester has strong robustness to n and ϖ. Some issues will arise when an over-long tether is used. One problem is that the cost will increase and the elastic tension within the tether will also increase (one can see this by observing the results in Fig. 6(a)). Moreover, perturbations by solar gravity will become significant.

Again, λ_{1I} is the imaginary part of the root of the characteristic equations of Eq. (25), and also the frequency of the damped oscillations as presented in Eq. (28). It is known that the system may be near resonance region when the frequency of the external load is near the damped frequency λ_{1I}. However, this is merely accurate for predicting the resonance region of linear dynamical systems and so there will exist deviations for predicting resonance regions of nonlinear dynamical systems. To show and clarify this, some analysis will be presented as follows.

Next, the points of peak power output obtained both numerically and analytically with η=4 and 2 are shown in Fig. 5(a). Figs. 5(b-d) show the peak points along each parameter set individually to explore how the peak power points vary with ϖ and n.

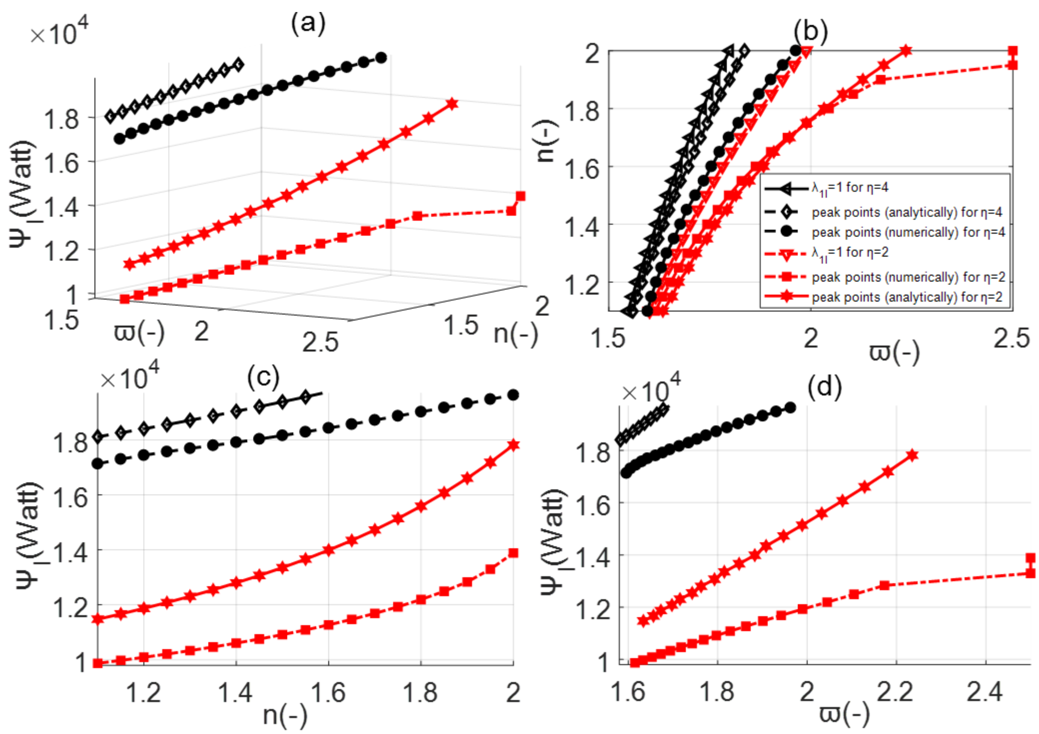

Fig. 5 **(a)** The peak points of power output for η=4 and 2; **(b-d)** the views from positive Ψ_l, ϖ and n directions respectively

It can be seen that the peak values for η=2 are smaller than those for η=4. Therefore, η=4 is adopted as an example of design of the tether system. Moreover, all peak points curves increase monotonically with n and ϖ as shown in Fig. 5(c-d). The power output predicted by the analytic solution is 21.48 kW when n=2 and ϖ=1.836 (i.e., the dimensional natural length, elasticity and damping are $l_0=1.297\times10^8$ m, $k=1.193297184\times10^{-5}$ N/m, and c_d=19.5475 N·s/m accordingly), compared to the numerical solution which yields 19.63 kW when n=2 and ϖ=1.963 (i.e., the dimensional natural length, elasticity and damping are $l_0=1.297\times10^8$ m, k= 1.364092626×10^{-5}

N/m, and c_d= 20.89966 N·s/m accordingly). Again, it is suggested that one should design a long tether, not only because the broad resonance region will ensure robustness as discussed previously, but also due to the increased power output. It is also found that λ_{I1}=1 (for both η=4 and 2) is near the peak points (for both analytical and numerical results) when the natural length and elasticity are small, as shown in Fig. 5(b). However, deviations will appear when the natural length and elasticity become larger. One can find the peak points roughly near λ_{I1}=1 and this provides an estimation to locate resonance peak points for preliminary analysis, although the deviations become evident when both the natural length and elasticity become large.

Next, the largest steady-state tension and elastic strain within the tether system are presented in Fig. 6, again shown together with the boundaries of the resonance region (red lines) and peak power curves (black lines) using numerical method as given in Fig. 6(a.1, b.1).

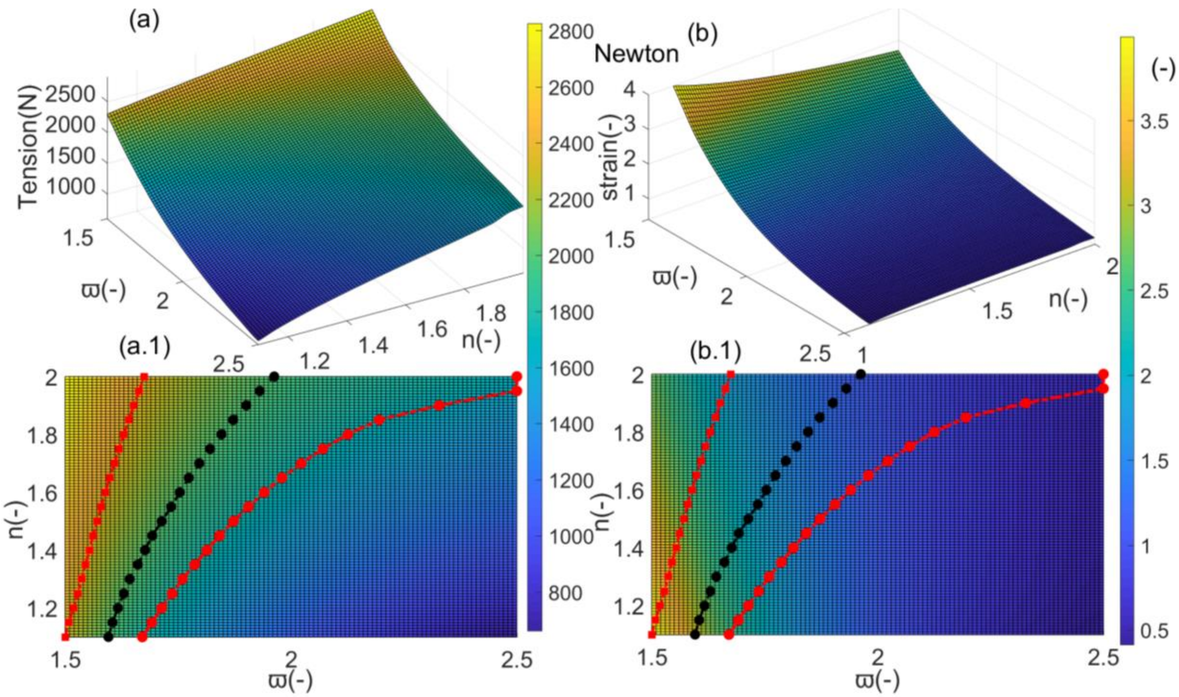

Fig. 6 **(a, a.1)** The largest steady tensions and **(b, b.1)** elastic strains within the space tether.

One can see that the largest steady-state tensions within the tether decrease and increase with ϖ and n from Fig. 6(a, a.1) respectively. Therefore, the smallest and largest tensions, approximately 660 N and 2800 N, can be found at the bottom right and top left up in Fig. 6(a, a.1) respectively. For the tension, it is suggested that one should select both large n and ϖ to harvest at high power output, but with relatively low tension. Therefore, it appears that the top right resonance region is preferred. The power outputs are found to be 18.37 kW and 19.63 kW when n=2, ϖ=1.963 and n=2, ϖ=2.5 respectively (the dimensional natural length, elasticity and damping are l_0=1.297×10^8 m, k=1.364092626×10^{-5} N/m and c_d= 20.89966 N·s/m, and l_0=1.297×10^8 m, k=2.2125×10^{-5} N/m and c_d= 26.61699 N·s/m respectively accordingly). It appears that the tension reduction is not significant when we select n=2 and ϖ=2.5 (tension is 1676 N) instead of n=2 and ϖ=1.963 (tension is 1996 N).

Furthermore, it also appears that the strain decreases with both n and ϖ from Fig. 6(b.1). In fact, it increases with n when ϖ is large (e.g., when ϖ=2.5), however, it appears that the strain is insensitive to changes in n and ϖ when ϖ is large (the right half of Fig. 6(b.1)). This implies that one can design an energy harvester with a high power output at the cost of increasing the tether strain. The strain approaches 1.119 at the largest power out (approximately 19.63 kW) when n=2, ϖ=1.963. If we select n=2, ϖ=2.5, the power output decreases to be 18.37 kW and the strain becomes 0.5806. This means that we may decrease the strain significantly at the expense of harvesting at somewhat lower power, which seems attractive. Therefore, one should make a compromise when designing the space tether system.

It has been clarified that the power output is determined by n, ϖ and η, i.e., the dimensionless natural length, elasticity and damping of the tether. One can imagine that there exists an optimal dimensionless damping η with certain values for $n \in [1.1, 2]$ and $\varpi \in [1.5, 2.5]$ (the corresponding dimensional natural length and elasticity are $l_0 \in [7.1335 \times 10^7$ m, 1.297×10^8 m] and $k \in [7.964 \times 10^{-6}$ N/m, 2.2125×10^{-5} N/m]) to maximise the power output. To find the optimal η with certain values for ϖ and n, some numerical calculation results similar to those in Fig. 4(b) are presented in Fig. 7(a, b, c, d, e and f) for η=4.5, 5, 5.5, 6, 6.5 and 7 respectively.

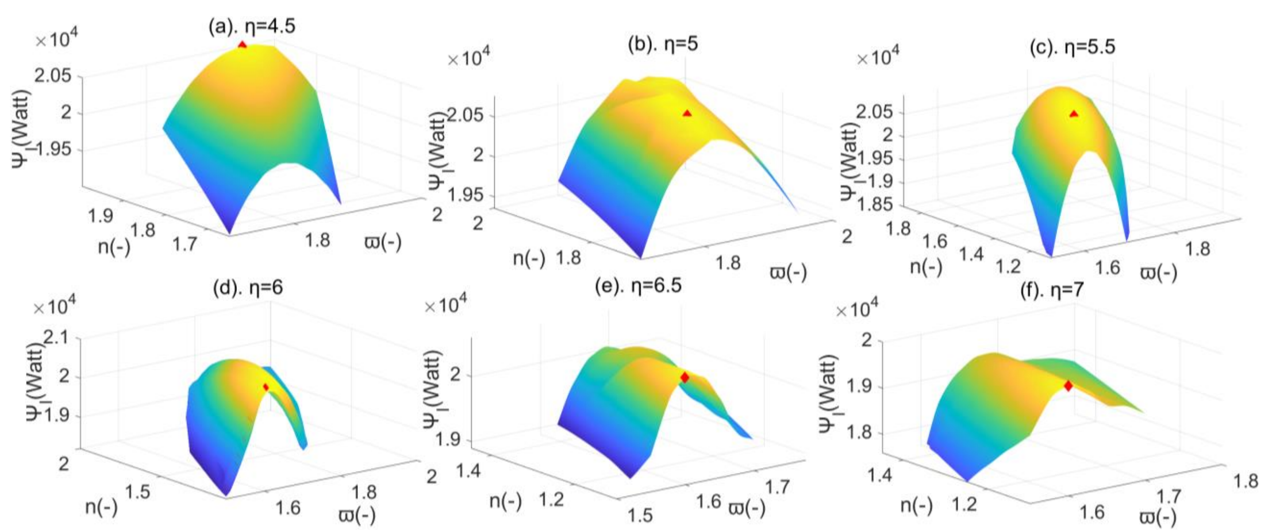

Fig. 7 (a-f). Power output based on the numerical method for η=4.5, 5, 5.5, 6, 6.5 and 7 respectively, the red diamonds correspond to the largest value

One can find the largest power output for each η, together with the corresponding ϖ and n. Similarly, one can also define resonance regions in each figure. It is advisable to select n and ϖ to ensure the space tether based energy harvester has some robustness. One could select n and ϖ at each diamond to make the power output maximum as long as the parameters can be kept fixed, without considering the robustness issue. If this is the case, one could summarize the largest power outputs and the corresponding natural length, elasticity and damping in the preceding figure in Table. 2.

Table 2. The largest power output for each damping and the corresponding natural length and elasticity of the tether

η/c_d(N·s/m)	ϖ/k(N/m)	n/l_0(m)	Ψ_l (Watt)
4/20.86772	$1.96/1.36\times10^{-5}$	$2.00/1.297\times10^{8}$	19630
4.5/23.3564	$1.95/1.346085\times10^{-5}$	$2.00/1.297\times10^{8}$	20490
5/24.6207	$1.85/1.211565\times10^{-5}$	$1.80/1.1673\times10^{8}$	20700
5.5/24.886886	$1.70/1.02306\times10^{-5}$	$1.40/9.079\times10^{7}$	20799
6/25.95	$1.625/9.3478125\times10^{-6}$	$1.15/7.45775\times10^{7}$	20847
6.5/27.68	$1.6/9.0624\times10^{-6}$	$1.1/7.1335\times10^{7}$	20548
7/29.811	$1.6/9.0624\times10^{-6}$	$1.1/7.1335\times10^{7}$	19977

It can be seen that the power output can be maximized (up to 20847 Watt) when η=6 is selected (the natural length and elasticity are 1.625 and 1.15 respectively), and the corresponding dimensional damping, elasticity and natural length are c_d=25.95 N·s/m, $k=9.3478125\times10^{-6}$ N/m and $l_0=7.45775\times10^{7}$ m respectively. It is interesting to note that the largest power output will move to smaller n and ϖ with the increment of η as observed in Table. 2. Compared to the results for η=4 with n=2 and ϖ =1.96 (i.e., c_d=20.86772 N·s/m, $k=1.36\times10^{-5}$ N/m and $l_0=1.297\times10^{8}$ m), one can harvest more power (20847 Watt) with a shorter tether (n=1.15 and $l_0=7.45775\times10^{7}$ m).

6. Conclusion

In this paper, energy harvesting analysis was performed for a massless viscoelastic tether connecting a tip mass to the Moon's surface. The tether in-plane librational and elongational motion (merely a planar problem was addressed) was obtained from the coupled dynamics and equilibria found which were used as reference positions to analyze the problem. To operate a space tether system successfully (such that the tether should be kept in tension), a large damping coefficient was adopted. The method of multiple scales was used to present approximate analytic solutions to the nonlinear dynamics with weak nonlinearity, was found to be effective to enable analytic results which were supported by numerical integration. It was concluded that the resonance regions of the tether system will move to lower frequencies when larger damping and a smaller tether length and elastic coefficient were adopted. The resonance regions become large when both the natural length and elasticity of the tether are large. For the power output obtained, the results indicated that one should select the peak power point when the dimensionless natural length of the tether denoted as n is 2 (the corresponding dimensional length is 1.297×10^{8} m). It was also concluded that one could find resonance regions roughly around the frequency of the damped system equal to the frequency of the external forcing due to the eccentricity of the Moon's orbit. It is suggested that one should design a tether-based lunar orbital energy harvester considering a compromise amongst cost, performance (including the power output and robustness of the harvester) and tension/strain when selecting the operating parameters. The optimal damping (η=6, c_d=25.95 N·s/m) was determined numerically, together with the corresponding natural length (n=1.15, l_0=7.45775×10^{7} m) and elasticity ($\varpi = 1.625$, k=9.3478125×10^{-6} N/m), for maximum power output (Ψ_l=20847 Watt). It was also interesting to note that a relatively high power output was available with a relatively short tether compared to the cases with smaller damping detailed in Table. 2.

In the future, one could focus on designing a space tether based energy harvester at L_1 and compared to the results at L_2 in this paper. Moreover, another interesting question is how to utilize nonlinear resonance to ascend a climber without consuming propulsions. Both will utilize gravitational tides to drive the system and make the system resonant.

Acknowledges

JL was support by NSFC (11302134) and China Scholarship Council program (201508210053). CM was support by a Royal Society Wolfson Research Merit Award. The authors would like to thank the reviewers and the Editor for their comments and constructive suggestions that helped to improve the paper significantly.

Appendix

In this appendix, the basic procedure for non-dimensionalisation is presented. The non-dimensionalisation procedure for the first four terms in Eq. (8) is taken as an example. The following basic equations/expressions are used for performing the non-dimensionalisation.

$$r = \frac{p}{1 + ecos\theta}, \dot{r} = \sqrt{\frac{\mu_a}{p}} esin\theta, \ddot{r} = \frac{\mu_a ecos\theta(1 + ecos\theta)^2}{p^2};$$

$$\dot{\theta} = \sqrt{\frac{\mu_a}{p^3}}(1 + ecos\theta)^2, \ddot{\theta} = -\frac{2\mu_a esin\theta(1 + ecos\theta)^3}{p^3} \tag{a.1}$$

The detailed non-dimensionalisation process for the first four terms in Eq. (8) is as follows utilizing Eq. (a.1).

$$\begin{aligned}
Term_{1-4} &= \ddot{l} + \frac{c_d}{m}\dot{l} + \frac{k}{m}(l - l_0) - l\dot{\theta}^2 \\
&= r\xi''\dot{\theta}^2 + 2\dot{r}\xi'\dot{\theta} + r\xi'\ddot{\theta} + \xi\ddot{r} + 2\eta\omega_n r\xi'\dot{\theta} + 2\eta\omega_n\xi\dot{r} + \omega_n^2\xi r - \omega_n^2\xi_0 r - \xi r\dot{\theta}^2 \\
&= \xi''(1 + ecos\theta)\underline{\frac{\mu_a}{p^2}(1 + ecos\theta)^2} + 2\xi' esin\theta\underline{\frac{\mu_a}{p^2}(1 + ecos\theta)^2} - 2\xi' esin\theta\underline{\frac{\mu_a}{p^2}(1 + ecos\theta)^2} \\
&+ \xi ecos\theta\underline{\frac{\mu_a}{p^2}(1 + ecos\theta)^2} + \frac{2\eta\xi'\varpi}{1 + ecos\theta}\underline{\frac{\mu_a}{p^2}(1 + ecos\theta)^2} + \frac{2\eta\xi\varpi esin\theta}{(1 + ecos\theta)^2}\underline{\frac{\mu_a}{p^2}(1 + ecos\theta)^2} \\
&+ \frac{\xi\varpi^2}{(1 + ecos\theta)^3}\underline{\frac{\mu_a}{p^2}(1 + ecos\theta)^2} - \frac{\xi_0\varpi^2}{(1 + ecos\theta)^3}\underline{\frac{\mu_a}{p^2}(1 + ecos\theta)^2} \\
&- \xi(1 + ecos\theta)\underline{\frac{\mu_a}{p^2}(1 + ecos\theta)^2}
\end{aligned} \tag{a.2}$$

where ω_n can be written as follows.

$$\omega_n = \frac{\omega_n}{\dot{\theta}}\dot{\theta} = \frac{\omega_n}{\sqrt{\frac{\mu_a}{p^3}}}\sqrt{\frac{\mu_a}{p^3}} = \varpi\sqrt{\frac{\mu_a}{p^3}}$$

Finally, the non-dimensional form for $Term_{1-4}$ can be given as follows by removing the underlined terms in Eq. (a.2). The final non-dimensional terms $Term'_{1-4}$ can be obtained as follows.

$$\begin{aligned}
Term'_{1-4} &= \xi''(1 + ecos\theta) + 2\xi' esin\theta - 2\xi' esin\theta + \xi ecos\theta + \frac{2\eta\xi'\varpi}{1 + ecos\theta} + \frac{2\eta\xi\varpi esin\theta}{(1 + ecos\theta)^2} + \frac{\xi\varpi^2}{(1 + ecos\theta)^3} \\
&- \frac{\xi_0\varpi^2}{(1 + ecos\theta)^3} - \xi(1 + ecos\theta) \\
&= \xi''(1 + ecos\theta) + 2\eta\varpi\frac{\xi esin\theta + \xi'(1 + ecos\theta)}{(1 + ecos\theta)^2} + \frac{\varpi^2(\xi - \xi_0)}{(1 + ecos\theta)^3} - \xi
\end{aligned} \tag{a.3}$$

Similarly, one can utilize the same procedure to perform the non- dimensionalisation for the remaining terms in Eqs. (8, 9).

Reference

[1] Rabl. Ari. Active solar collectors and their applications. Oxford University Press on Demand, 1985.

[2] Steven R. Anton, Daniel J. Inman. Vibration energy harvesting for unmanned aerial vehicles. Proc. SPIE 6928, Active and Passive Smart Structures and Integrated Systems 2008, 692824 (April 04, 2008); doi:10.1117/12.774990

[3] Sasaki, S., Tanaka, K., Higuchi, K., Okuizumi, N., Kawasaki, S., & Shinohara, N., et al. (2007). A new concept of solar power satellite: tethered-sps. Acta Astronautica, 60(3), 153-165.

[4] Mcinnes, C. R., Gorman, D. G., & Cartmell, M. P. (2008). Enhanced vibrational energy harvesting using nonlinear stochastic resonance. Journal of Sound & Vibration, 318(4), 655-662.

[5] A. Subin Das, B. Santhosh., Energy Harvesting from Nonlinear Vibration Absorbers. Procedia Engineering, Volume 144, 2016, Pages 653-659

[6] Cartmell, M. P., & Mckenzie, D. J. (2008). A review of space tether research. Progress in Aerospace Sciences, 44(1), 1-21.

[7] Zhong R., Zhu Z.H., Optimal current switching control of electrodynamic tethers for fast deorbit, Journal of Guidance, Control, and Dynamics, Vol. 37, No. 5, p. 1501-1511, 2014. DOI: 10.2514/1.G000385

[8] Wen, H., Zhu, Z.H., Jin, D.P., Hu, H.Y., Model Predictive Control with Output Feedback for a Deorbiting Electrodynamic Tether System, Journal of Guidance, Control, and Dynamics, Vol. 39, No. 10 (2016), pp. 2455-2460. https://doi.org/10.2514/1.G000535

[9] Cartmell, M.P. and Ziegler, S.W., ‘Experimental scale model testing of a motorised momentum exchange propulsion tether’, in: 37th AIAA/ASME/SAE/ASEE Joint Propulsion Conference and Exhibit, AIAA 2001-3914, Salt Lake City, Utah, U.S.A., 2001.

[10] Ziegler, Spencer W. The Rigid-body Dynamics of Tethers in Space. PhD Dissertation, University of Glasgow, 2003.

[11] Cartmell, M. and McInnes, C.R. and McKenzie, D. (2004) Proposals for an Earth-Moon mission design based on motorised momentum exchange tethers. In: Proceedings of the XXXII Summer School on Advanced Problems in Mechanics, APM 2004, St Petersburg. IPME RAS.

[12] Murray, C., & Cartmell, M. P. (2013). Moon-tracking orbits using motorized tethers for continuous Earth–Moon payload exchanges. Journal of Guidance, Control, and Dynamics, 36(2), 567-576.

[13] Burov, A. A., Guerman, A. D., & Kosenko, I. I. (2015). Uniform rotations of tethered system connected to a Moon surface. Acta Astronautica, 116, 349-354.

[14] Burov, A. A., Guerman, A. D., & Kosenko, I. I. (2014). Tether orientation control for lunar elevator. Celestial Mechanics and Dynamical Astronomy, 120(3), 337-347.

[15] Jin, D.P., Wen, H.: Nonlinear resonance of a subsatellite on a short constant tether. Nonlinear Dyn. 71(3), 479–488 (2013)

[16] Pang, Z., Jin, D., Yu, B., & Wen, H. (2016). Nonlinear normal modes of a tethered satellite system of two degrees of freedom under internal resonances. Nonlinear Dynamics, 85(3), 1779-1789.

[17] Daqaq, M. F., Masana, R., Erturk, A., and Quinn, D. D., 2014, “On the Role of Nonlinearities in Vibratory Energy Harvesting: A Critical Review and Discussion,” ASME Appl. Mech. Rev., 66(4), p. 040801

[18] Wei Yang, Shahrzad Towfighian. Internal resonance and low frequency vibration energy harvesting. Smart Materials and Structures, 26 (9) (2017)

[19] Wei Yang, Shahrzad Towfighian. A hybrid nonlinear vibration energy harvester. Mechanical Systems and Signal Processing, Volume 90, June 2017, Pages 317-333

[20] Rodrigo T. Rocha, Jose M. Balthazar, Angelo M. Tusset, et al. Nonlinear piezoelectric vibration energy harvesting from a portal frame with two-to-one internal resonance. Meccanica, September 2017, Volume 52, Issue 11–12, pp 2583–2602

[21] Chunbo Lan, Weiyang Qin, Wangzheng Deng. Energy harvesting by dynamic unstability and internal resonance for piezoelectric beam. Appl. Phys. Lett. 107, 093902 (2015); https://doi.org/10.1063/1.4930073

[22] Xu, J., & Tang, J. (2015). Piezoelectric Cantilever-pendulum for Multi-directional Energy Harvesting with Internal Resonance. Proc. of SPIE (Vol.107, pp.197-205).

[23] Karimpour, H., & Eftekhari, M. (2014). Exploiting internal resonance for vibration suppression and energy harvesting from structures using an inner mounted oscillator. Nonlinear Dynamics, 77(3), 699-727.

[24] Harne, R. L., & Wang, K. W. (2013). A review of the recent research on vibration energy harvesting via bistable systems. Smart Materials & Structures, 22(2), 023001.

[25] Avvari, P. V., Tang, L., & Soh, C. K. (2013). Enhancement of piezoelectric energy harvesting with multi-stable nonlinear vibrations. Proceedings of SPIE - The International Society for Optical Engineering, 8688(3), 108-111.

[26] Cottone, F., Gammaitoni, L., Vocca, H., Ferrari, M., & Ferrari, V. (2012). Piezoelectric buckled beams for random vibration energy harvesting. Smart Materials & Structures, 21(3), 035021.

[27] Cottone, F., Basset, P., Vocca, H., Gammaitoni, L., & Bourouina, T. (2013). Bistable electromagnetic generator based on buckled beams for vibration energy harvesting. Journal of Intelligent Material Systems & Structures, 25(12), 1484-1495.

[28] Hao Peng, Xiaoli Bai, Shijie Xu. (2018). Continuation of periodic orbits in the Sun-Mercury elliptic restricted three-body problem. Commun Nonlinear Sci Numer Simulat 47 (2017) 1-15

[29] Hao Peng, Xiaoli Bai. Natural deep space satellite constellation in the Earth-Moon elliptic system. Acta Astronautica, in press,(2017).

[30] M. Cartmell, Introduction to Linear, Parametric, and Nonlinear Vibrations, Chapman & Hall, London, 1990.

[31] A. Nayfeh, D.T. Mook. Nonlinear Oscillations. Wiley, New York (1979)